

Effect of Heat Treatment and La Doping on the Electrical Properties of BiFeO₃

Fazal Ullah¹, M.S. Awan², Z. Wazir¹, Irfan Sabir³, A. ul Haq¹

¹Department of Physics, Faculty of Engineering and Applied Sciences,
Riphah International University, I-14, Islamabad 44000, Pakistan.

²Ibn-e-Sina Institute of Science and Technology (IIST), H-11/4, Islamabad 44000, Pakistan.

³Department of Electrical Engineering, Bahria University, Islamabad 44000, Pakistan.

anwar.haq@riphah.edu.pk*

(Received on 7th December 2017, accepted in revised form 12th March 2018)

Summary: La doped phase-pure multiferroic BiFeO₃ (BFO) was prepared by the co-precipitation method using precursor bismuth oxide and iron nitrate Nona hydrate. The pallets of pure BFO were sintered in the temperature range from 500 to 650 °C for 1h in air. The structure of as-synthesized powders and pallets were studied by Powder X-ray diffraction method. Surface morphology was characterized by the Field Emission Scanning Electron Microscope and their dielectric properties were investigated as a function of sintering temperature and La doping. The DC electrical resistivity as a function of temperature was also measured. It is concluded that optimum sintering temperature is 500 °C to obtain pure phase of BFO. The grain size of the pallets was found to increase as a function of sintering temperature for the samples whereas grain size has decreased as a function of La doping. The pallets of both pure and La doped samples exhibited high AC resistivity, dielectric constant and low dielectric loss values.

Key Words: BiFeO₃, La-doping, Co-Precipitation Method, Sintering, Electrical properties, Scanning Electron Microscopy, X-ray Diffraction

Introduction

Materials that possess magneto-electric coupling between ferroelectric and ferromagnetic orders are called multiferroic materials. These materials have charming fundamental physics and numerous industrial applications so they have attracted many researchers [1-11]. These ferroic orders hardly coexist due to three-dimensional (3D) orbital electronic structure, being essential for magnetism and to reduce the tendency for ferroelectricity [1]. These systems are infrequent in nature. The examples of such systems are found in the perovskite oxides like YMnO₃, BiMnO₃ and BiFeO₃ (BFO). BFO is a single phase multiferroic material at room temperature. It is G-type antiferromagnetic and its Curie and Neel temperature is of the order of 820 and 370 °C, respectively [2]. These materials have intrinsic coupling between the electric polarization and magnetic moments due to which one may write data electrically and then read magnetically. As such these materials may play a vital role in the next generation memory devices. Sensors, optoelectronic devices, satellite communications, optical filters, electrically tunable ferromagnetic resonance devices, spintronic etc. are some of the interesting applications of multiferroic materials [3, 4].

The crystal structure of BFO is distorted perovskite pseudo cubic with space group R3c [5].

Along their body diagonal [111] direction, the two perovskite pseudo-cubic aligns to form rhombohedra, which then combines to form a hexagonal unit cell. The rotation of the oxygen octahedral is clock and anticlock wise around the [111] direction alternatively. There is a spin cyclical order with a period of 64 nm which is superimposed on this antiferromagnetic order. The weak ferromagnetism at room temperature is due to the spin canting in antiferromagnetic BFO. However, the spin cycloid averages out the macroscopic magnetization. The energy of the BFO unit cell can be lowered by off centering the bismuth ions with respect to the neighboring oxygen ions. The intrinsic electric polarization is due to the displacement of bismuth cations relative to the Fe-O₆ octahedral [7].

The synthesis of single-phase BFO ceramics is difficult due to the peculiar thermodynamic and kinetic properties of Bi₂O₃-Fe₂O₃ system [8-12]. Practical applications of BFO in industry are slowed down due to the formation of secondary phases during the synthesis process of BFO and volatile nature of Bi at elevated sintering temperatures. The conversion of Fe⁺³ into Fe⁺² and formation of oxygen vacancies are the main cause of leakage current that affect the conductivity of BFO [8]. The achievement of superior multiferroic order in BFO is difficult, due to the impurity phases such as Bi₂₅FeO₃₉, Bi₂Fe₄O₉,

*To whom all correspondence should be addressed.

Fe_2O_3 and Bi_2O_3 [9]. Numerous and often unsuccessful attempts have been made using a variety of different processing methods. In addition to the conventional solid-state method, there are many reports on hydrothermal synthesis, sol-gel, rapid liquid-phase sintering, mechano-chemical synthesis, precipitation method, combustion synthesis and high-pressure synthesis. Yao et al. [13] used solid state reaction method etc. to prepare the BFO but they could not avoid the formation of secondary phases. Bernardo et al. [14] investigated the structural and microstructural properties by using the doping of e.g. W^{6+} , Nb^{5+} and Ti^{4+} in BFO. Ding et al. [15] studied the structural and microstructural properties of Ti-La co-doping in the BFO above 850 °C. Garcia-Zaleta et al. [16] prepared La doped BFO by Pechini method. The effect of La doping on phase formation, grain size, electric and magnetic properties was investigated. They reported decrease in grain size and increase in electrical and magnetic properties due to La doping. You et al. [17] prepared La doped highly strained thin films of BFO with coexistence of tetragonal-like and rhombohedral-like phases. Peng-Ting et al. [18] prepared La doped BFO by sol-foam-gel method and observed that La doping results change in crystallographic structure of BFO from rhombohedral to Tetragonal. They concluded that La doping increased ferromagnetism due to breaking of spin cycloid structure. The aim of this work is to synthesize the phase pure BFO and study the effect of heat treatment and La doping on the grain size and AC electrical properties.

Experimental

The multiferroic bismuth ferrite was synthesized through co-precipitation method [19]. This method is environmental friendly, cost effective and does not need high temperature for synthesis as compared to other methods. As a first step appropriate amount of analytical grade bismuth oxide; Bi_2O_3 (98% pure) was dissolved in 63 wt. % HNO_3 and analytical grade iron nitrate Nona hydrate; $\text{Fe}(\text{NO}_3)_3 \cdot 9\text{H}_2\text{O}$ (99.99% pure) in deionized water separately to get 0.4 M ionic solutions and were homogenized by stirring for 30 minutes. An aqueous solution of molarity 1 M of sodium hydroxide was also prepared in deionized water. In second step ionic solutions of bismuth oxide and iron nitrate were mixed and quickly sodium hydroxide solution was added to get precipitates. The pH value of 12 was maintained to facilitate the phase purity and small grain size of the Bi ferrite [19]. The temperature of the solution was increased to 80 ± 2 °C and maintained for 45 minutes under continuous stirring at room temperature for 30 minutes for better

homogenization. In the third step, the precipitates were washed with the deionized water to remove impurities till we get pH 7 of the solution. The separated precipitates were dried in an oven at 100 °C for overnight. The acquired substance was ground into fine powder by mortar and pestle. The as-synthesized powder was amorphous bismuth ferrite, BiFeO_3 (BFO), which was used for further studies. The as-synthesized BFO powder is denoted as S. The digits after S denote calcination temperature. For example S350 stands for as-synthesized sample calcined at 350 °C. To prepare La doped samples, lanthanum oxide was dissolved into 63% nitric acid by replacing bismuth in the 0.1, 0.2, 0.3 and 0.4 molar ratios. Rest of the procedure was the same as mentioned above. In this case product was $\text{Bi}_{1-x}\text{La}_x\text{FeO}_3$, where $x = 0.1-0.4$ mol. %. The La doped samples are denoted by BLFO. For phase formation and crystallization, the BFO samples were calcined at 350–550 °C for 1 h in the steps of 50 °C. The powder samples were uniaxially pressed at a pressure of 20 MPa to make pallets of 12 mm diameter and 1.5 mm thickness. The BFO pallets were sintered from 500 to 650 °C for one hour in the steps of 50°C. The BFO pallets are denoted by P. The digits after P indicate sintering temperature. For example P500 stands for BFO pallet sintered at 500 °C. Since best structure and pure phase for BFO was obtained at 500 °C, therefore the La doped pallets were sintered only at 500 °C. La doped pallets are denoted by P. The digits after P indicate concentration of La for example P0.1 denote BFLO pallet with 0.1 % La.

For structural studies, Cu source in X-Ray generator model PAN analytical, X' Pert Pro was used. The X-ray tube was operated at 40 keV and 30 mA. Ni filter was used to get Cu-K α radiation. Lattice constant was calculated by iterative method using software called "unit cell". Field Emission Scanning Electron Microscope (FESEM) of HITACHI SU-1500 was used to find the surface morphology and grain size of the samples. LCR Meter of Wayne Kerr Precision Component Analyzer Model 6440B was used to measure the dielectric properties at room temperature in the frequency range from 20Hz to 3MHz and DC electrical resistivity from room temperature to 300 °C for all the sintered pallets by two probe methods. Pressure contacts, equal to the pallet size were used after polishing the surfaces. The dielectric constant was calculated from the equation [11]:

$$\epsilon = Cd / \epsilon_0 A$$

Where A is the cross-sectional area of the pallet, d is the thickness of the pallet, C is the Capacitance and ϵ_0 is the permittivity of free space. The values of dielectric constant (ϵ') and dielectric loss tangent [tan

(δ)] at the same frequency range can be used to calculate the AC conductivity by using the following relation [6]: $\sigma_{AC} = \omega \epsilon_0 \epsilon' \tan(\delta)$. Where σ_{AC} is the AC conductivity and ω is the angular frequency.

Results and Discussion

The XRD patterns of all the samples were taken from 2θ values of 15 to 75° . Fig.1A shows the XRD patterns for as-synthesized powder as a function of calcination temperature for the BFO samples. This figure shows the XRD patterns of as-synthesized powder denoted by S. There is only one broad peak registered which indicate that samples are mainly amorphous. However, the sample S450 which was calcined at 450°C and shown in Fig.1A, indicated that BFO phase has now started recrystallizing and there is one sharp peak at around 2θ value of 31° and six other peaks which have low intensities. All peaks were labeled by comparing XRD data with Joint Committee on Powder Diffraction Standards (JCPDS) cards number 00-014-0181. All these peaks could be indexed as hexagonal lattice of Bi ferrite. Since intensities of the peaks were low we now increased calcination temperature to check if this would help to improve crystallization. The XRD pattern of sample S500 is also shown in Fig.1A, indicated that intensities have increased somewhat and again all peaks could be indexed according to the hexagonal lattice. To improve further recrystallization, temperature for calcination was further raised to 550°C . But to our surprise, a very small impurity peak in x-ray diffraction pattern at 2θ value of 28.7° (sample S550) appeared, which indicate that some impurity phase has started developing.

Since we want to study electrical properties of the pure Bi ferrite phase, therefore the powder calcined at 500°C was used to make 5 pallets as described above. These pallets were sintered at 500, 550, 600 and 650°C for one hour in each case to study the effect of sintering temperature on the recrystallization behavior of BFO. These samples are denoted by P. For each sintering temperature a new pallet was used.

Fig.1B shows x-ray patterns of sintered pallets. All the diffraction peaks for sample P500 could be indexed as per JCPDS cards no. 00-014-0181 for the hexagonal lattice and there was no impurity peak Thus it is pure BFO phase. As the sintering temperature is increased to 550°C (see Fig 1B), the impurity peaks started developing.

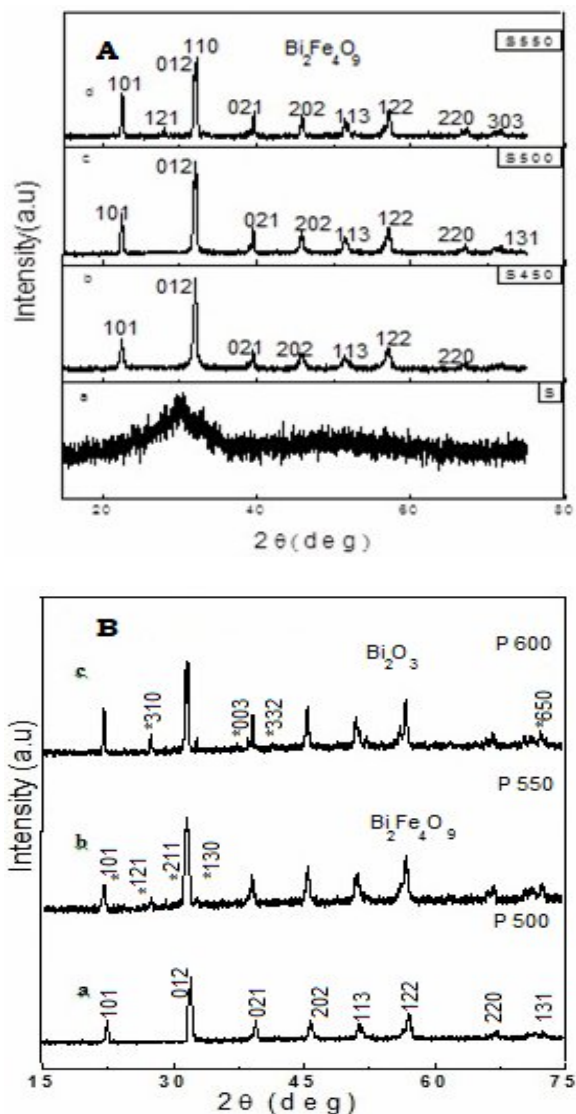


Fig. 1: (A) XRD pattern of BFO (BiFeO_3) as synthesized (S) and calcined at (S350)- 350°C , (S400)- 400°C , (S450)- 450°C , (S500)- 500°C , (S550)- 550°C for one hour in each case. -(B) shows the XRD pattern of BFO (BiFeO_3) pallets sintered at (P500)- 500°C , (P550)- 550°C , (P600)- 600°C and (P650)- 650°C . * $\text{Bi}_2\text{Fe}_4\text{O}_9$ and + Bi_2O_3

Impurity peaks of $\text{Bi}_2\text{Fe}_4\text{O}_9$ and BiFeO_3 phase are visible. At 600°C (P600) more impurity peaks appeared. When sample is sintered at 650°C , it develops predominantly $\text{Bi}_2\text{Fe}_4\text{O}_9$ phase and only one peak of BiFeO_3 was observed as such its diffractogram is not presented. Non-perovskite phases such as Bi_2O_3 and $\text{Bi}_2\text{Fe}_4\text{O}_9$ were observed at higher sintering temperature i.e. $\geq 500^\circ\text{C}$. These impurity phases are formed possibly due to volatility of Bi^{3+} ions and creation of oxygen vacancies and

conversion of Fe^{3+} to Fe^{2+} ions [20]. Thus it is confirmed that 500 °C is the optimum sintering temperature to get phase pure Bi ferrite. It is also noted that peak full width half maximum (FWHM) appears to decrease with increasing sintering temperature due to increase in grain size.

Table-1 presents the lattice parameters and unit cell volume as a function of sintering temperature for the hexagonal lattice. It may be noted that lattice parameter “a” and “c” remain constant as a function of sintering temperature up to 600 °C but at sintering temperature 650 °C, lattice parameter “c” has increased significantly thereby increasing cell volume also. Fig. 2A shows the x-ray diffraction patterns as a function of La doping in BFO. It can be seen from this figure that doping of La up to 0.4% keeps the rhombohedral lattice intact [21]. Some variations in the 2θ values as compared to the sample P500 are noted. Table 2 shows the lattice parameters and cell volume of La doped samples. It is worth mentioning that lattice parameter “a” remains almost constant. But lattice parameter “c” has decreased significantly resulting decrease in cell volume.

Table-1: Lattice parameters of BFO as a function of sintering temperature.

# pallets	a (Å)	c (Å)	V (Å) ³
P500	5.56	13.93	373.01
P550	5.57	13.91	373.15
P600	5.57	13.91	373.94
P650	5.54	14.24	378.53

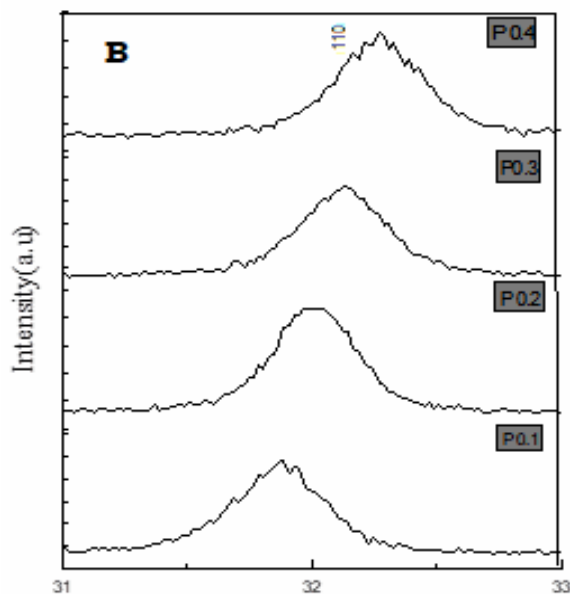
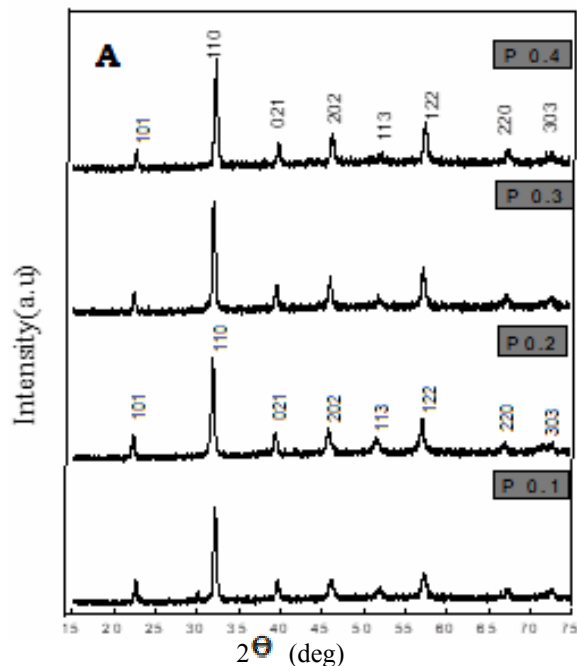


Fig. 2: (A) XRD pattern of the La doped BLFO pallets sintered at 500 °C (P0.1) 0.1 La, (P0.2) 0.2 La, (P0.3) 0.3La and (P0.4) 0.4 La concentration. -(B) The magnified (101) peak of XRD pattern of La doped pallets sintered at 500°C (P0.1) 0.1 La, (P0.2) 0.2 La, (P0.3) 0.3 La and (P0.4) 0.4 concentration.

Fig.2B shows the magnified view of (110) peak appearing at $2\theta = 32.5^\circ$ for La doped samples. It may be noted that (110) peak shows some shifting at higher angle side due to increase in La doping. This indicate that La^{3+} ions have replaced the Bi^{3+} ions effectively with small decrease in the lattice parameters as the ionic radius of La^{3+} (0.116pm) is smaller than ionic radius of Bi^{3+} (0.117 pm) without significantly distorting the lattice of BFO [22]. In the case of La doping although (110) peak has shifted to higher 2θ values but no peak split is observed. This leads us to conclude that La doping helps to retain rhombohedral structure. This is in contradiction to the literature [23, 24]. Table-2 shows the lattice parameters and cell volume of La doped samples. It is worth mentioning that lattice parameter “a” remains almost constant. But lattice parameter “c” has decreased significantly resulting decrease in cell volume.

Table-2: Lattice parameters of BLFO as a function of La concentration.

#pallets	a (Å)	c (Å)	V (Å) ³
P0.1	5.56	13.95	374.05
P0.2	5.55	13.81	368.20
P0.3	5.56	13.81	369.50
P0.4	5.55	13.57	361.57

Microstructural Analysis

FESEM is used to study the surface morphology and grain size distribution in sintered pure BFO and BLFO pellets. Fig. 3 shows the surface morphology and grain structure of BFO pellets as a function of sintering temperature. It is seen that grains which were predominantly spherical in P500 sample have

changed their shape to rectangular in P550. Furthermore the grain growth has also been observed as sintering temperature is increased. The average grain size for the sample P500 was 560 ± 77 nm which increased to 707 ± 113 nm for the sample P650 as shown in the Fig. 3A and Fig 3D, respectively. It is known that large grains show better electrical conductivity [11].

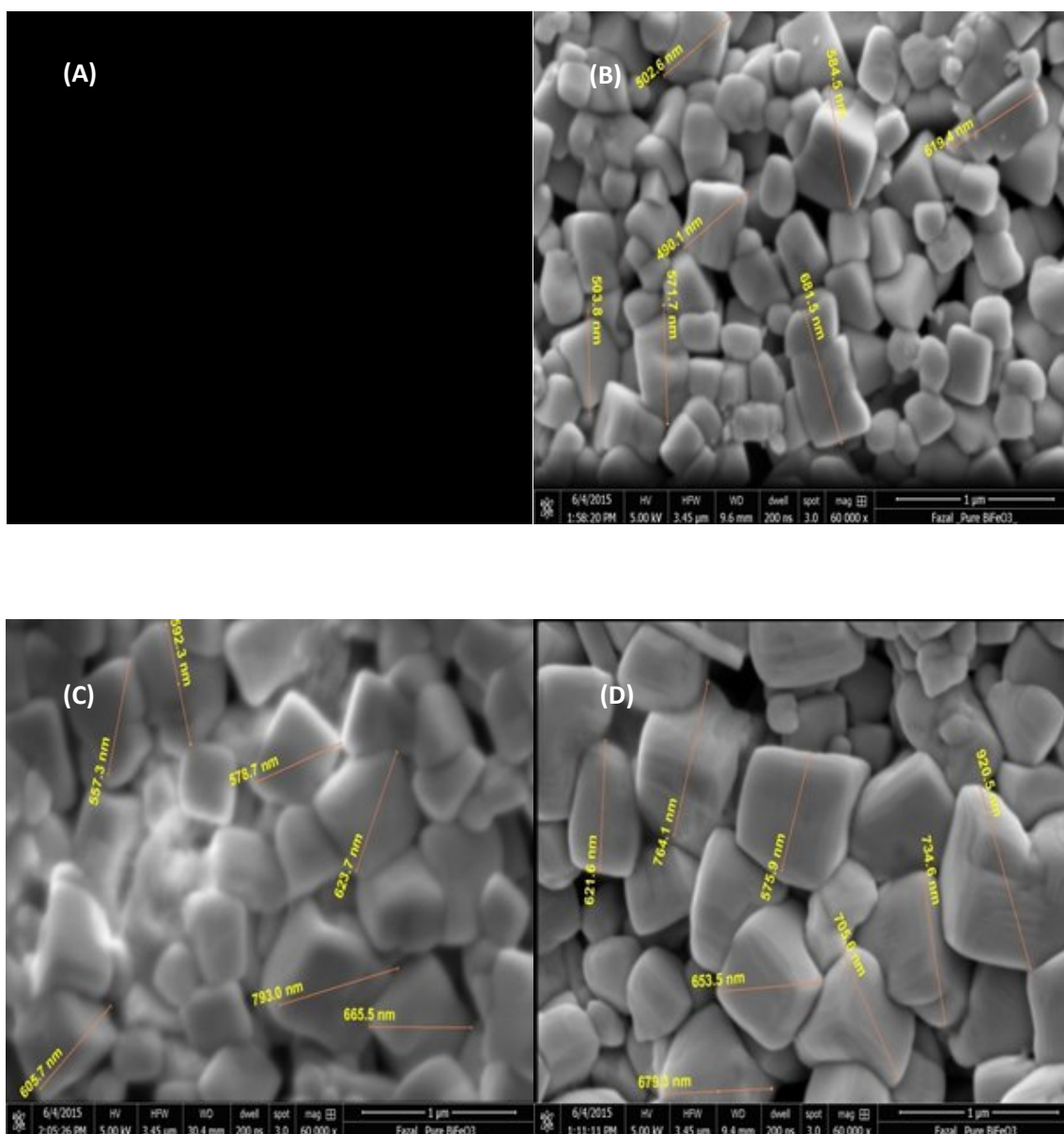


Fig. 3 SEM micrographs of BFO pellets as a function of sintering temperature, A- (P500-500 °C), B- (P550-550 °C), C- (P600-600 °C) and D- (P650-650 °C)

Fig. 4 presents the SEM micrographs of La doped BFO samples. It is worth to note that the grain size of pure BFO sintered at 500 °C is large as compared to the BLFO. The comparison of Fig 3 and 4 shows that the average grain size of BFO is decreasing as the concentration of La is increasing. The average grain size for P0.1 (Fig 4A) was 87 ± 30 nm which decreased to 37 ± 23 nm for the sample P0.4 (Fig 4D). This leads us to conclude that the grain

growth is suppressed by the rare earth ions especially manganite's whose base is rare earth [25]. It is stated in the literature that oxygen vacancies formation in BFO may be suppressed by the doping of La. The motion of oxygen ion will be slow if the oxygen vacancies are less which in turn will lead to low grain growth rate [26]. It is also noted that FWHM of the La doped samples increased with increasing La concentration due to decrease in grain size.

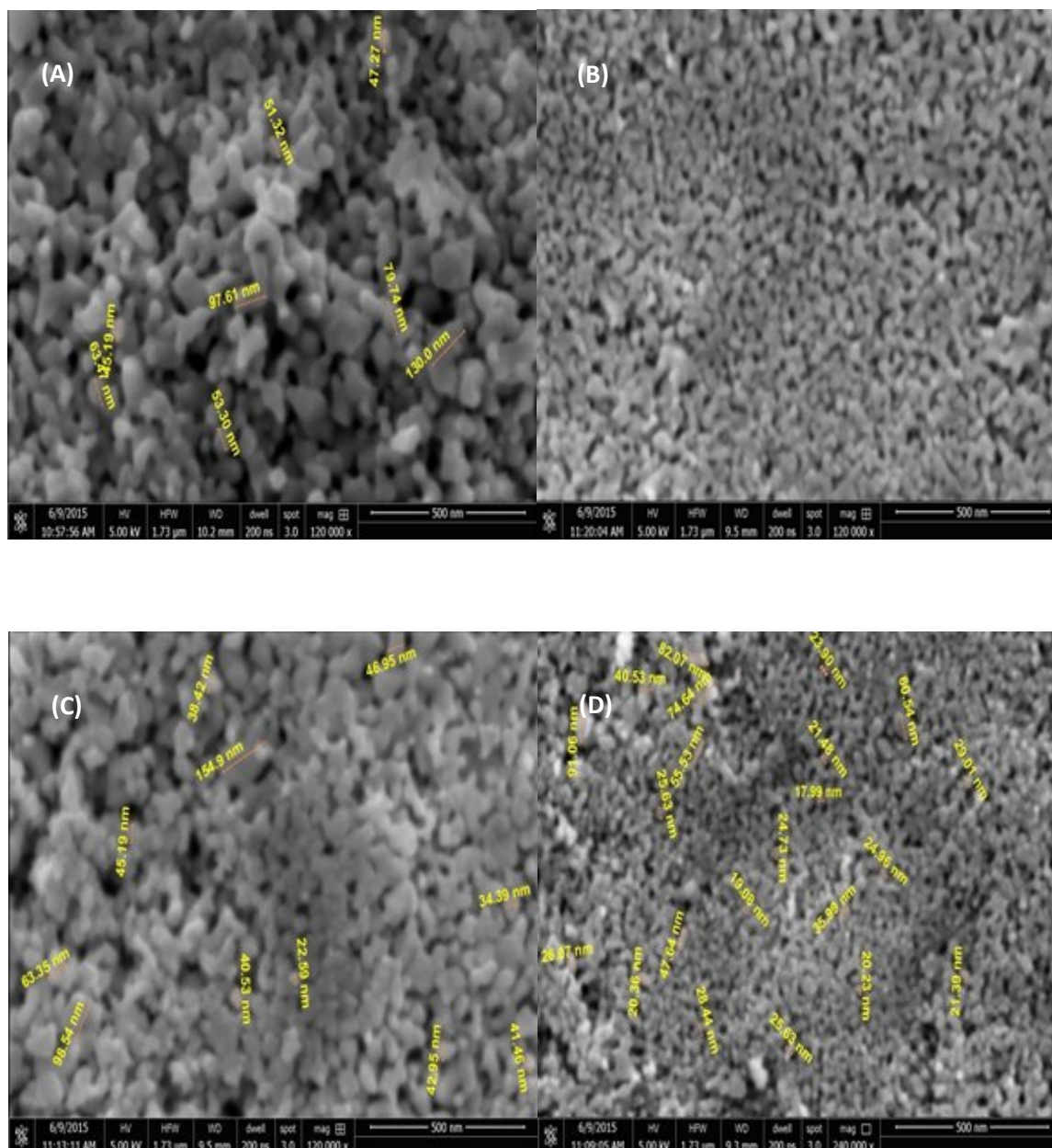


Fig. 3: SEM micrographs of BFO pallets as a function of sintering temperature, A (P500-500 °C), B (P550-550 °C), C (P600-600 °C) and D (P650-650 °C).

Growth is suppressed by the rare earth ions especially manganite's whose base is rare earth [25]. It is stated in the literature that oxygen vacancies formation in BFO may be suppressed by the doping of La. The motion of oxygen ion will be slow if the oxygen vacancies are less which in turn will lead to low grain growth rate [26]. It is also noted that FWHM of the La doped samples increased with increasing La concentration due to decrease in grain size.

DC Electrical Resistivity

Fig. 5A shows the plot of DC electrical resistivity as a function of temperature for the sintered BFO samples. It is observed that room temperature resistivity of BFO was in the range of $G\Omega\cdot\text{cm}$ which decreased to the $M\Omega\cdot\text{cm}$ range with increasing sintering temperature. This decrease in resistivity is possibly due to the decrease in porosity, good connection among grain boundaries, formation of conduction ions, the impurity phases and grain coarsening at higher sintering temperatures. All samples manifested semiconducting behavior. Fig.5B shows the Arrhenius plot of data presented in Fig.

5A. The activation energy for pallets of BFO named P500, P550, P600 and P650 was calculated and it is 0.868eV, 0.525eV, 0.6177eV and 0.6291eV, respectively. Fig. 6A shows the resistivity of La doped samples as a function of temperature up to 300 °C. As expected it is observed that increasing in La doping has resulted increase in the resistivity values. Here again the resistivity values are in $G\Omega\cdot\text{cm}$ range at room temperature. All the four samples follow the same trend. The room temperature resistivity values of the BLFO samples are higher as compared to the BFO samples. This may be due to its smaller grain size of BLFO samples and increased grain boundary scattering [21]. The DC resistivity in BLFO samples also show semiconducting behavior. This may be due to fact that charge carriers are assisted thermally and tunneled through grain boundaries transport mechanism of polaron hopping and electrons thermally activated to the conduction band [27]. Fig.6B shows the Arrhenius plot of the data presented in Fig. 6A. The activation energy for the pallets of BLFO samples named P0.1, P0.2, P0.3 and P0.4 was calculated and these are 0.5359eV, 0.4630eV, 0.5647eV and 0.6496eV, respectively.

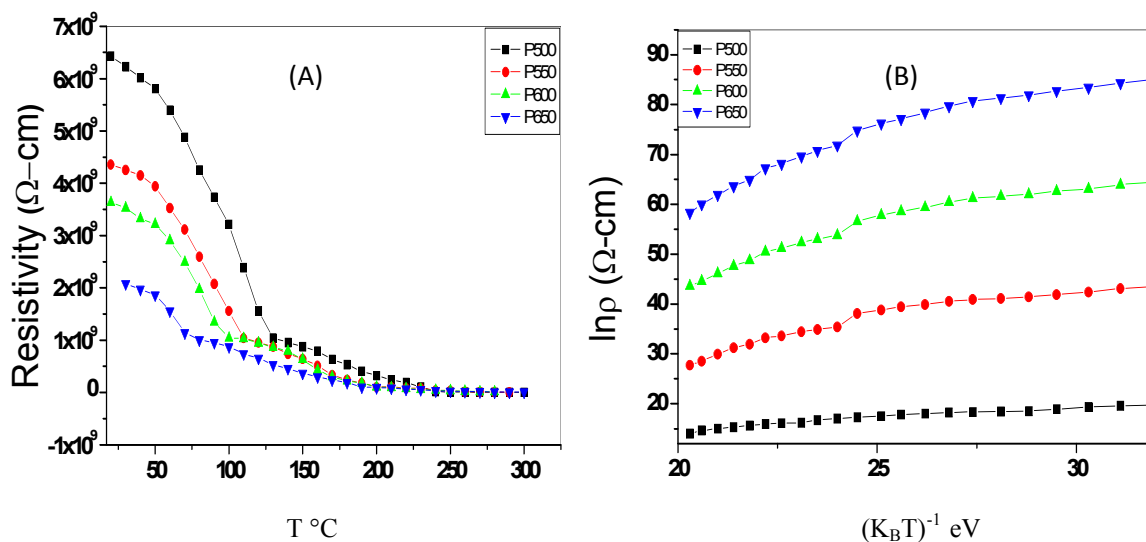


Fig. 5: (A) The DC electrical resistivity of pure sintered pallets of P500 (500 $^{\circ}\text{C}$), P550 (550 $^{\circ}\text{C}$), P600 (600 $^{\circ}\text{C}$) and P650 (650 $^{\circ}\text{C}$) -(B) The Arrhenius plot for sintered pallets of BFO; P500, P550, P600, P650.

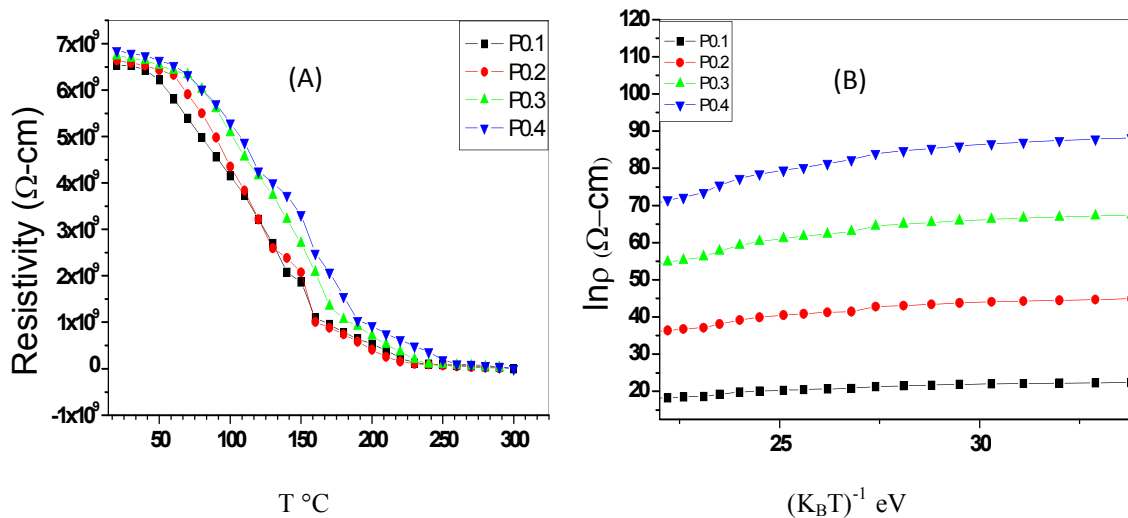


Fig. 6: (A) The DC electrical resistivity of BLFO sintered pallets P0.1, P0.2, P0.3 and P0.4; -(B) The Arrhenius plot of sintered pallets of BLFO; P0.1, P0.2, P0.3 and P0.4.

Dielectric Properties

Dielectric properties such as the dielectric loss [$\tan(\delta)$], dielectric constant (ϵ') and AC conductivity (σ) for all pure BFO and BLFO sintered pallets were measured at room temperature by parallel-plate method, in the frequency range from 20 Hz to 3 MHz and are presented in the Figs. 7 and 8. In the case of BFO (Fig.7A) there is only one relaxation peak in the frequencies range of 20 Hz to 1 kHz. But in the case of BLFO (Fig.8A), there are two relaxation peaks for the dielectric loss tangent. First peak is in the frequencies range of 20 Hz to 1 kHz. The second peak is in the frequencies range of 10 to 100 kHz. The first peak may be due to the contribution of electric dipole, electrons, ions and space charge. As the frequency increased from 10 Hz to 100 Hz, space charge does not have enough time to build up interfacially and undergo first relaxation [11]. The dipole moment do not have sufficient time to align along the applied varying field at high frequencies as there is no relaxation peak so their contribution dies out for pure BFO [28]. In the case of BLFO, La plays a vital role in the dielectric loss. La ions tend to decrease the crystallite size which leads to increase resistivity values. There is more grain boundary scattering in a material containing more small grains which leads to enhance electrical resistivity and hence leading to low dielectric loss [30].

It is observed that sample P650 (BFO) exhibited maximum value of dielectric constant of 150. This may be due to the excess of free ions, well connected grain walls, high density and low porosity values. A sharp decrease in the values of dielectric constant is noted in all the BFO and BLFO pallets as a function of frequency up to 1 kHz (see Fig.7B and Fig.8B). The dielectric constant at 50 Hz for P0.4 (BLFO) is more than that of P0.1 (BLFO). This is attributed to the crystallite size [31]. The sharp decrease in the dielectric constant may be due to the decrease in interfacial polarization which may be explained by Maxwell-Wagner model for polarization [29].

It can be seen from Fig.7C that σ_{AC} for the BFO increased as a function of frequency. Koop's model [30] predicts that by increasing the sintering temperature there will be increase in the electrical conductivity. According to Koop's model, polycrystalline materials consist of well-defined conducting grains with resistivity, ρ_g and thickness, t_g . These are separated by poor conducting grain boundaries with resistivity, ρ_{gb} and thickness t_{gb} . The electrical resistivity for such materials is given by: $\rho_s = \rho_g + (t_{gb}/t_g) \rho_{gb}$. Maxwell-Wagner model may be used to explain this behavior. The grain boundaries will shrink and grain thickness will increase when the sintering temperature is increased. Therefore, the electrical AC conductivity of the samples will enhance with the decrease in (t_{gb}/t_g) value.

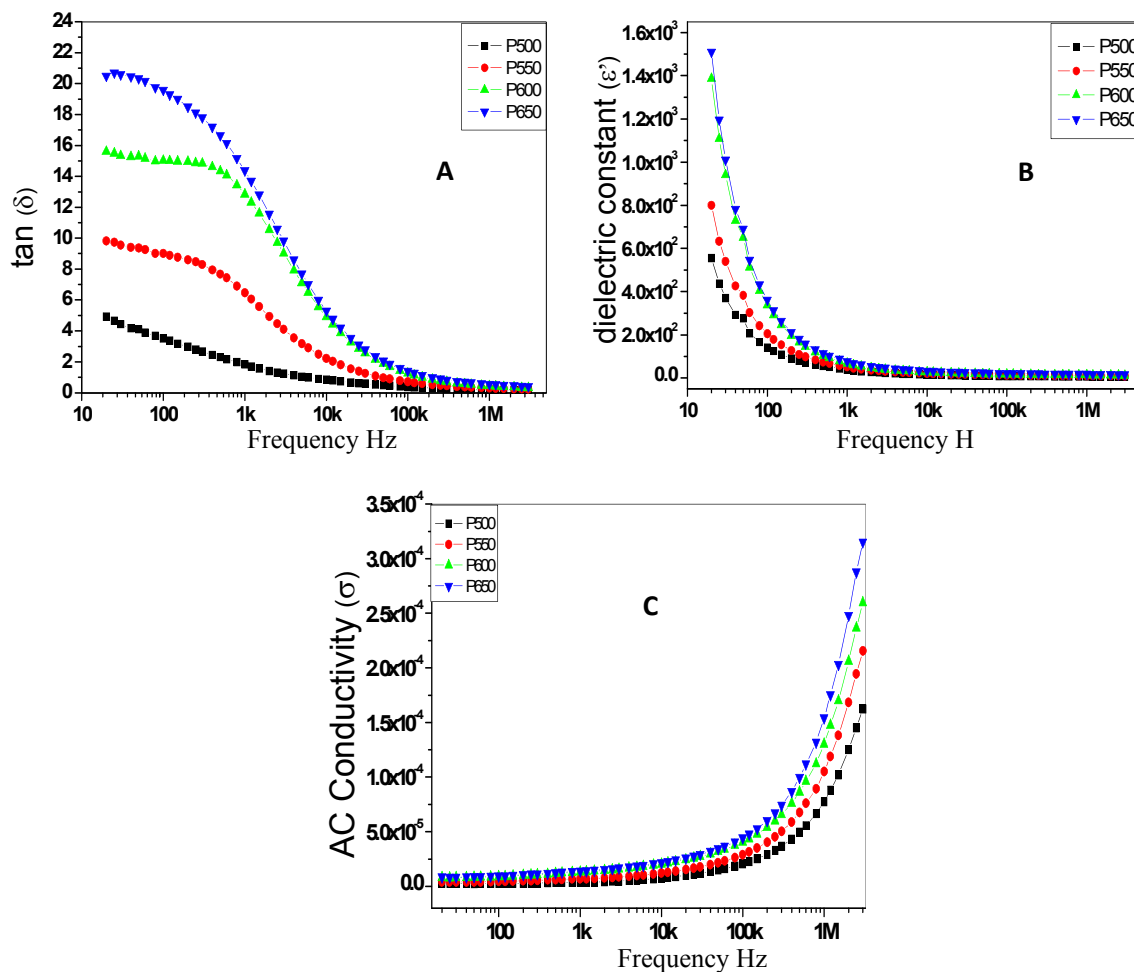
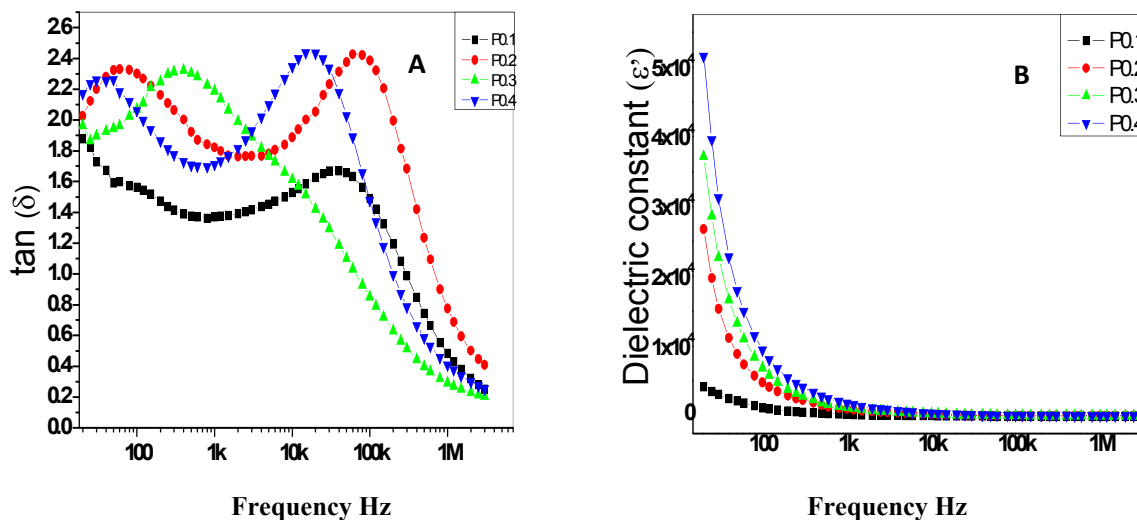


Fig. 7: (A) Dielectric loss of BFO sintered pallets P500, P550, P600 and P650. (B) Dielectric constant of BFO sintered pallets P500, P550, P600 and P650. (C) AC Conductivity of BFO sintered pallets P500, P550, P600 and P650



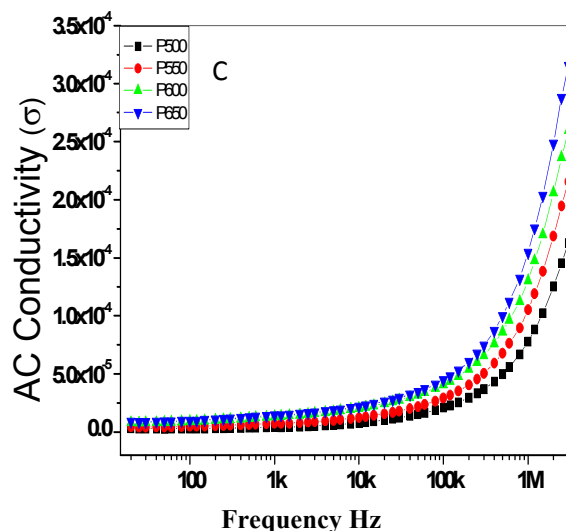


Fig. 8: (A) Dielectric loss of BLFO sintered pallets P0.1, P0.2, P0.3 and P0.4. -(B) Dielectric constant of BLFO sintered pallets P0.1, P0.2, P0.3 and P0.4. -(C) AC Conductivity of BLFO sintered pallets P0.1, P0.2, P0.3 and P0.4

The AC conductivity for all the BLFO samples are the same in the low frequency range of 20-1kHz as shown in the Fig.8C. Beyond the 1 kHz the σ_{AC} value increased sharply. The concentration of the La plays an important role in the AC conductivity in the frequency range above 1MHz. The AC conductivity of P0.4 is less than the P0.1 which indicates that their leakage current will be very low in that region and probably the nanoparticles would have caused this low conductivity [31]. This low value of AC conductivity for P0.4 is due to the small grain size of the P0.4 sample as compared to P0.1 sample. Smaller grain size material will have more grain boundaries as compared to the large grain size material. Thus scattering of electron from the grain boundaries will be more in the smaller grains material as compared to large grains material resulting in high resistivity and hence low conductivity and hence low leakage current [32].

Conclusions

Phase pure multiferroic BiFeO_3 nanopowder has been synthesized by simple coprecipitation method at a temperature, as low as 500 °C. Precursor Bi_2O_3 played an important role in avoiding the impure phases. Amorphous nature and phase purity of BFO has been confirmed by XRD analysis. It is concluded that grain size increased with the increase in sintering temperature of pure BFO. Whereas the grain size decreased with the increase in doping of La. Sintering temperature above 550 °C resulted development of impurity phases. The sintering temperature and La doping influenced the

dielectric behavior as a function of frequency, showing one relaxation peak for dielectric dispersion. For the resistivity as a function of temperature, all the samples showed semiconducting trend following Arrhenius behavior. Whereas in the case of La doped samples, the lattice constants and grain size of the samples are found to decrease with the increase of La doping. Enhanced dielectric properties are observed for the doped counterparts of BFO nanoparticles. It is evident from the studies that the incorporation of La has been effective in refining the microstructure; reducing the oxygen vacancies, lower grain growth rate which leads to reduce the electrical conductivity.

References

1. C. H Wang, Z. F Liu, L. Yu, Z. M. Tian and S. L. Yuan Structural, magnetic and dielectric properties of $\text{Bi}_{5-x}\text{LaTi}_3\text{Co}_{0.5}\text{Fe}_{0.5}\text{O}_{15}$ ceramics, *Mater. Sci. Eng.* **B176**, 1243 (2011).
2. V. S. Puli, A. Kumar, N. Panwar, I. Panwar and R. S. Katiyar, Transition metal modified bulk BiFeO_3 with improved magnetization and linear magneto-electric coupling, *J. Alloys Compd.*, **509**, 8223 (2011).
3. Z. Wen, L. You, X. Shen, X. Li, D. Wu, J. Wang and A. Li, Multiferroic properties of $(\text{Bi}_{1-x}\text{Pr}_x)(\text{Fe}_{0.95}\text{Mn}_{0.05})\text{O}_3$ thin films, *Mater. Sci. Eng.*, **B176**, 990 (2011).
4. G. Biasotto, A. Z. Simoes, C. R. Foschini, M. A. Zaghete, J. A. Varela and E. Longo, Microwave-hydrothermal synthesis of perovskite bismuth ferrite nanoparticles, *Mater. Res. Bull.* **46**, 2543 (2011).

- K. Liu, H. Fan, P. Ren, and C. Yang, Structural, electronic and optical properties of BiFeO₃ studied by first-principles, *J. Alloys Compd.* **509**, 1901 (2011).
- D. Varshney, A. Kumar, and K. Verma, Effect of A site and B site doping on structural, thermal, and dielectric properties of BiFeO₃ ceramics, *J. Alloys Compd.* **509**, 8421 (2011).
- X. Zhang, Y. Sui, X. Wang, J. Mao, R. Zhu, Y. Wang and Z. Wang, Bi_{0.85}La_{0.1}Ho_{0.05}FeO₃ ceramics, *J. Alloys Compd.* **509**, 5908 (2011).
- A. Kumar and K. L. Yadav, Magnetic, magneto-capacitance and dielectric properties of Cr doped bismuth ferrite nano-ceramics, *Mater. Sci. Eng.* **B176**, 227 (2011).
- Z. M. Tian, Y. S Zhang, S. L Yuan, M. S Wu, C. H Wang, Z. Z. Ma, S. X Huo, and H. N. Duan, Enhanced multiferroic properties and tunable magnetic behavior in multiferroic BiFeO₃-Bi_{0.5}Na_{0.5}TiO₃ solid solutions, *Mater. Sci. Eng.* **B177**, 74 (2012).
- H. Ke, W. Wang, Y. Wang, Jiahuan Xu, Dechang Jia, Zhe Lu and Yu Zhou, Factors controlling pure-phase multiferroic BiFeO₃ powders synthesized by chemical co-precipitation, *J. Alloys Compd.* **509**, 2192 (2011).
- M. Y. Shami, M. S. Awan and M. Anis-ur-Rehman, Phase Pure Synthesis of BiFeO₃ Nanopowders Using Diverse Precursor via Co-Precipitation Method, *J. Alloys Compd.* **509**, 10139 (2011)
- T. Rojac, A. Bencan, B. Malic, G. Tutuncu, Jacob L. Jones, John E. Daniel and D. Damjanovic, BiFeO₃ Ceramics: Processing, Electrical, and Electromechanical Properties, *J. Am. Ceram. Soc.* **97** 1993 (2014).
- Y. Yao, B. Ploss, C.L. Mak, and K.H. Wong, Pyroelectric properties of BiFeO₃ ceramics prepared by a modified solid, *Appl. Phys.* **A99**, 211 (2010)
- M.S. Bernardo, T Jardiel, M. Peiteado, A.C. Caballero and M. Villegas, Sintering and microstructural characterization of W⁶⁺, Nb⁵⁺ and Ti⁴⁺ iron-substituted BiFeO₃, *J. Alloys Compd.* **509**, 7290 (2011)
- Y. Ding, T.H. Wang, W.C. Yang, T.C. Lin, C.S. Tu, Y.D. Yao and K.T. Wu, Magnetization, Magnetoelectric Effect, and Structure Transition in BiFeO₃ and (Bi_{0.95}La_{0.05}) FeO₃ Multiferroic Ceramics, *IEEE Trans. Mag.* **47**, 513 (2011)
- D.S. Garcia-Zaleta, A.M. Torres-Huerta, M.A. Dominguez-Crespo, J.A. Matutes-Aquino, A.M. Gonzalez and M.E. Villafuerte-Castrejon, Solid solutions of La-doped BiFeO₃ obtained by the Pechini method with improvement in their properties, *Ceram. Intern.* **40**, 9225 (2014)
- L. You, P. Caesario, L. Fang, L. Wang, Y. Zhou, A. Gruverman and J. Wang, Effects of BaCu(B₂O₅) addition on sintering temperature and microwave dielectric properties of Ba₅Nb₄O₁₅-BaWO₄ ceramics, *Physical Review* **B90**, 13410 (2014)
- P.T. Li, X. Li, Z. Li, J.H. Yin, X.W. Cheng, Z.H. Wang, Y.C. Wu and G.H. Wu, *Chin. Phys.* **B23**, 047701 (2014)
- M. Srivastava, A.K. Ojha, S. Chaubey, P.K. Sharma and A.C. Pandey, Influence of pH on structural morphology and magnetic properties of ordered phase cobalt doped lithium ferrites nanoparticles synthesized by sol-gel method, *Mater. Sci. Eng.* **B175**, 14 (2010)
- P. Pandit, S. Satapathy and P.K. Gupta, Effect of La substitution on conductivity and dielectric properties of Bi_{1-x}La_xFeO₃ ceramics: An impedance spectroscopy analysis, *Phys.* **B406**, 2669 (2011)
- A.S. Priya and I.B. Shameem Banu, Effect of doping and annealing on the room temperature magnetic and dielectric properties of La modified BiFeO₃ multiferroic nanoparticles synthesized by sol-gel citrate combustion method, *Int. J. Chem. Tech Res.* **6**, 4643 (2014)
- F. Gonzalez-Garcia, C.S. Riccardi and A.Z. Simões, Lanthanum doped BiFeO₃ powders: Syntheses and characterization, *J. Alloys Compd.* **501**, 25 (2010)
- X. Yan, J. Chen, Y. Qi, J. Cheng and Z. Meng, Hydrothermal synthesis and characterization of multiferroic Bi_{1-x}La_xFeO₃ crystallites, *J. Eur Ceram. Soc.* **30**, 265 (2010)
- H. Ke, W. Wang, Y. Wang, J. Xu, D. Jia, Z. Lu and Y. Zhou, Factors controlling pure-phase multiferroic BiFeO₃ powders synthesized by chemical co-precipitation, *J. Alloys Compd.* **509**, 2192 (2011)
- A. Azam, A. Jawad, A.S. Ahmed, M. Chaman and A.H. Naqvi, Structural, optical and transport properties of Al³⁺ doped BiFeO₃ nanopowder synthesized by solution combustion method, *J. Alloys Compd.* **509**, 2909 (2011)
- T. Soitah and C. Yang, Effect of Fe³⁺ doping on structural, optical and electrical properties δ-Bi₂O₃ thin films, *Curr. Appl. Phys.* **10**, 724 (2010)
- R. C. Kambale, P. A Shaikh, C. H. Bhosale, K. Y. Rajpure and Y. D. Kolekar, Studies on magnetic, dielectric and magnetoelectric behavior of (x) NiFe_{1.9}Mn_{0.1}O₄ and (1-x) BaZr_{0.08}Ti_{0.92}O₃ magnetoelectric composites, *J. Alloy Compd.* **489**, 310 (2010)

28. D. Zanghuai and Y. Akishige, Electrical properties of multiferroic BiFeO₃ ceramics synthesized by spark plasma sintering, *J. Phys.* **D43**, 445403 (2010)
29. G. Catalan, Magnetocapacitance without magnetoelectric coupling, *Appl. Phys. Lett.* **88**, 102902 (2006)
30. C Koops, On the dispersion of resistivity and dielectric constant of some semiconductors at audiofrequencies, *Phys. Rev.* **83**, 121 (1951)
31. M. Hojamberdive, Y. Xu, F. Wang, W. Liu and J. Wang, La-modification of multiferroic BiFeO₃ by hydrothermal method at low temperature, *Inorg. Mater.* **45**, 1183 (2009)
32. G. kumar, S. sharma, R.K. Kotnala, J. Shah, S. E. Shirsath, M.K. Batoo and M. Singh, Electric, dielectric and ac electrical conductivity study of nanocrystalline cobalt substituted Mg–Mn ferrites synthesized via solution combustion technique, *J. Mol. Structure*, **1051**, 336 (2013)